ACS OMEGA

http://pubs.acs.org/journal/acsodf

Article

Synthesis and Characterization of a Novel Quaternary Ammonium Salt as a Corrosion Inhibitor for Oil-Well Acidizing Processes

Zaidoun K. Kuraimid, Dawood S. Abid, and Abd El-Aziz S. Fouda*

Cite This: *ACS Omega* 2023, 8, 27079−27091

Read Online

ACCESS | Metrics & More | Article Recommendations

ABSTRACT: A quaternary ammonium salt, 1,1′-(1,4-phenylenebis-(methylene))bis(4-formylpyridin-1-ium) (PMBF), was synthesized, characterized, and investigated as an inhibitor for C1018 (type steel in oil wells) corrosion in 17.5% HCl solution. The chemical structure of PMBF was confirmed using altered techniques. Potentiodynamic polarization (PDP) was employed to investigate the corrosion inhibition effect of the synthesized compound in a 17.5% HCl solution for C1018. The corrosion protection was increased by improving the dose of the synthesized compound and reached 98.5% at 42.02 × 10^{-5} M and 313 K. On the other hand, it was decreased by increasing the temperature and reached 97.9% at the same concentration and 343 K. The parameters of activation and adsorption were calculated and debated. A polarization study revealed that PMBF functioned as a "mixed-kind inhibitor," i.e., affecting both cathodic and anodic processes through their adsorption onto the electrode surface. The adsorption was described by the Langmuir adsorption isotherm. Different techniques were employed as appropriate tools for analyzing the structure of the layer formed on C1018. Density functional theory (DFT) and Monte Carlo (MC) simulations were used to compare the results of the theoretical calculations with the experiments. Finally, an appropriate inhibition mechanism was suggested and discussed.

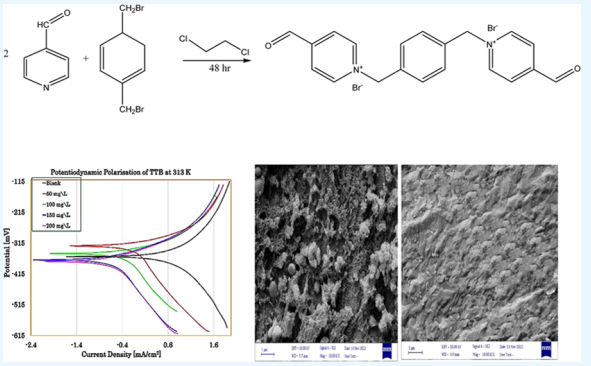

1. INTRODUCTION

In several industrial sectors, acid solutions are typically used to remove undesired scales and rust from steel surfaces. They are also frequently employed to improve oil and gas recovery through acidification in the oil and gas industry.[1]

These processes generally cause substantial corrosion of steel pipes, tubes, and equipment.[2] The presence of mineral acid solutions, which are utilized as aggressive solutions for pickling,[3] cleaning,[4] descaling,[5] and oil-well acidization,[6] is a vital phenomenon for carbon steel corrosion. However, adding corrosion inhibitors in very little amounts will minimize the negative effects of corrosion caused by the acids.[7] An important role in preventing corrosion is played by corrosion inhibitors.[8] Literature indicates that the presence of heteroatoms like nitrogen, oxygen, sulfur, and phosphorus in organic compounds can be effective in reducing the corrosive attack on metal surfaces by aggressive species.[9] Organic compounds containing heteroatoms act at the interface between the metal and corrosive solution by adsorbing onto the metal surface. This adsorption results in the formation of a protective layer that isolates the metal surface from the corrosive environment.[10] The reason for selecting a quaternary ammonium salt with incorporated hetero-organic moieties in this study is that they have greater potential to protect steel against corrosion. This is due to the presence of heteroatoms that can form a protective layer on the metal surface.[11] It has been discovered that organic corrosion inhibitors with nitrogen reduce hydrogen's ability to penetrate steel in acid conditions.[12]

As corrosion inhibitors for mild steel in 15% HCl at 105 °C, Quraishi et al.[13] synthesized two undecane-5-mercapto-1-oxa-3,4-diazole (UMOD), two heptadecane-5-mercapto-1-oxa-3,4-diazole (HMOD), and two decane-5-mercapto-1-oxa-3,4-diazole (DMOD). Inhibition tests were also carried out on N-80 steel under similar conditions in 15% HCl containing 5000 ppm of UMOD. According to the data, oxadiazole derivatives are effective corrosion inhibitors. N-80 steel has 94% inhibition effectiveness according to UMOD, whereas mild steel had 72% inhibition efficiency. PDP tests performed on mild steel in 15% HCl with 500 ppm oxadiazole derivatives and on N-80 in 15% HCl with 500 ppm UMOD at room temperature revealed that all of the chemicals under investigation are mixed-type inhibitors. Frenier et al.[14] studied two model compounds, *n*-dodecylpyridinium bromide (*n*-

Received: March 29, 2023
Accepted: June 19, 2023
Published: July 21, 2023

Scheme 1. PMBF Inhibitor's Synthesis Route

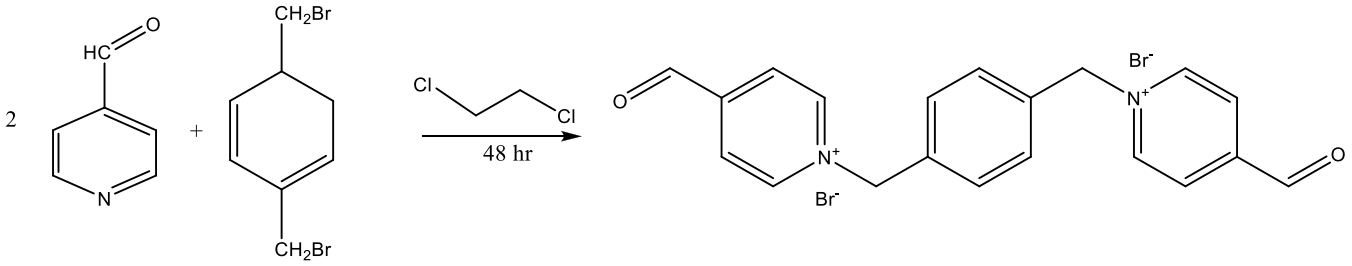

DDPB) and 1-octyn-3-ol, that were tested in HCl acid as inhibitors for J55 oilfield steel. This paper describes the kinetic and chemical analyses conducted to arrive at inhibition mechanisms for these model compounds. These studies showed that the pyridinium forms a weak bond with the chloride-covered surface and is sensitive to temperature and [HCl]. Octynol, however, chemisorbs and produces a film that contains a reaction product of acetylenic alcohol. The efficiency of the newly created chemical, 6-methyl-5-[*m*-nitro styryl], was evaluated by Migahed et al.[15] as a corrosion inhibitor for mild steel in 12% HCl solution at 50 °C by employing a variety of chemical and electrochemical methods. Zhang et al.[16,17] looked into the efficacy of three quaternary ammonium salts as corrosion inhibitors for Q235 steel, including tetradecyl trimethyl ammonium bromide, *N*-benzyl pyridinium chloride, and imidazoline quaternary ammonium salt. The corrosion rate was greatly reduced, and the findings showed good inhibitory efficiency. Also observed by Zhang et al.[18] was the synergistic corrosion inhibition effect of octadecylamine and tetradecyl trimethyl ammonium bromide at concentrations of 10 and 20 mg L^{-1}, respectively. Jalab et al.[19] investigated the corrosion performance of quaternium-22 (Q-22) surfactant ($C_{13}H_{29}N_2ClO_7$) in 5 M HCl solution against C1018 and obtained 51% inhibition efficiency at 2.22 mmol L^{-1}, 30°C. Wang et al.[20] utilized phenacyl quinolinium bromide (PaQBr) and DiPaQBr (classified as an indolizine quaternary ammonium salt) as inhibitors for N-80 steel in 17.5% HCl and obtained inhibition efficiencies of 97.7% and 97.1% at 35.6 mM and 25 °C, respectively. Hegazy et al.[21] synthesized and characterized three novel diquaternary ammonium salts, namely, *N*-(3-(2-(isopropyldimethylammonio)acetoxy)propyl)-*N*,*N*-dimethyldodecan-1-aminium chloride bromide (Q1), *N*-(3-(2-((2-hydroxyethyl) dimethylammonio) acetoxy) propyl)-*N*,*N*-dimethyldodecan-1-aminium chloride bromide (Q2), and *N*-(3-(2-(phenyldiethylammonio)acetoxy)propyl)-*N*,*N*-dimethyldodecan-1-aminium chloride bromide (Q3) and utilized them as corrosion inhibitors for API X65 steel pipeline in 1 M HCl. The inhibition efficiencies for these Q1, Q2, and Q3 were 97, 98, and 99.5% at 20 °C and 5×10^{-3} M, respectively.

The goal of the study is to synthesize and characterize a novel quaternary ammonium salt named (PMBF) and test its effectiveness as a corrosion inhibitor in oil wells where acid injection occurs. Due to its charged structure, the PMBF with high solubility, high molecular size, nontoxicity, and easy preparation is considered safe for the environment and displays efficient adsorption behavior. Both WL and PDP were used to assess the % IE. Several kinetic and thermodynamic parameters were computed using the experimental data. The surface morphology of the C1018 alloy corroded in 17.5% HCl with and without the addition of the inhibitor was examined using atomic force microscopy (AFM) and scanning electron microscopy (SEM) techniques.

2. EXPERIMENTAL SECTION

2.1. Materials. α,α'-Dibromo-*p*-xylene was purchased from BDH, 1,2-dichloroethane was purchased from Merck, 4-pyridyne carboxaldehyde was purchased from Macklin, and hydrochloric acid was purchased from J Baker. All of these reagents are of analytical reagent (AR) grade. The corrosion inhibitor synthesized in this manuscript was dissolved in water. We prepared a 10,000 ppm stock solution by dissolving 1 g of inhibitor in 100 mL of water.

2.2. Synthesis of 1,1′-(1,4-Phenylenebis(methylene))-bis(4-formylpyridin-1-ium) (PMBF).[22] In a round-bottomed flask, a magnetic stirrer was equipped. The mixture consisting of α,α'-dibromo-*p*-xylene (0.05 mole) (13.19 g = 9.42 mL) and 4-pyridyne carboxaldehyde (0.1 mole) (10.71 g) in 1,2-dichloroethane was refluxed for 48 h. After cooling, the solvent was removed. The separated solid was filtered and purified. The light-yellow solid gave a yield of 91%; MP 115.3 °C.

2.3. Composition of C1018 Alloy. A C1018 steel coupon with an area of 1 cm^2 was used as the working electrode for the polarization method. Its composition was C 0.17%, Mn 0.8%, P 0.014%, S 0.002%, Si 0.022%, Cu 0.02%, Ni 0.01%, Cr 0.04%, Sn 0.002%, Ti 0.001%, Cd 0.001%, V 0.001%, B 0.0001%, Al 0.042%, N 0.006%, and the remainder being Fe. Specimens were cleaned in accordance with ASTM standard G1-3[24] before the start of any experiment.

2.4. PDP Studies (Tafel Extrapolation). Electrochemical experiments were performed using a potentiostat device winking MLab-200(2007) (Bank Elektronik - Intelligent Controls GmbH) and a glass-jacketed cell with three electrodes. As an auxiliary electrode, the platinum over titanium (Pt/Ti) electrode was utilized and the reference electrode was made of silver over silver chloride (Ag/AgCl). Tafel extrapolation was used to calculate corrosion rates. The experiments were carried out at altered temperatures (313–343 K) in accordance with ASTM standards G-01 and G-05.[23] The experiments were performed at least three times to check the reproducibility.

2.5. Surface Characterization. C1018 samples used for surface analysis were submerged at 313 K for 3 h in extract-free acid and acid containing 42.02×10^5 M PMBF. After that, the samples were removed, cleaned with double distilled water many times to remove any residue, and dried. The surface morphologies of C1018 samples were determined by a FESEM Instrument ZEISS Sigma VP, Iran, Tehran. Atomic force microscopy (AFM, with high-resolution type) measurements were performed by a NaioAFM 2022, Nanosurf, Switzerland at the Iraqi Ministry of Industry, Baghdad, Iraq.

https://doi.org/10.1021/acsomega.3c02094
ACS Omega 2023, 8, 27079−27091

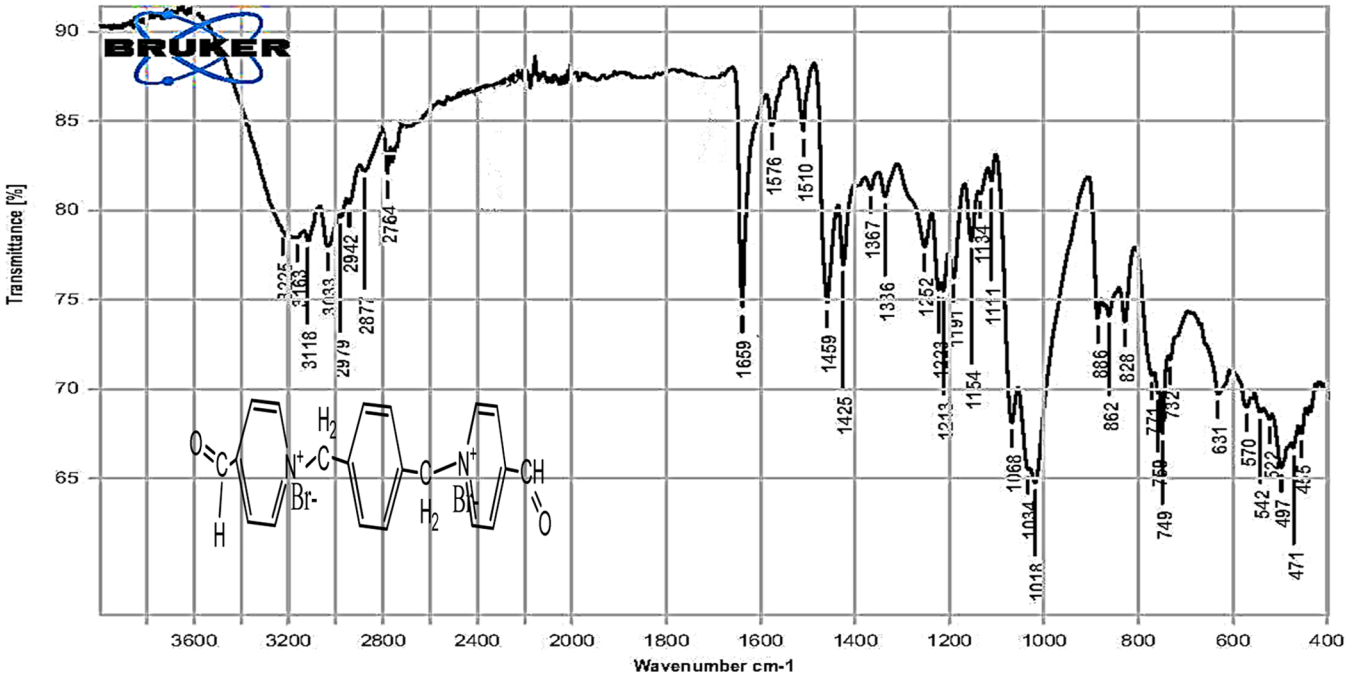

Figure 1. FT-IR spectrum of PMBF.

Table 1. Spectral Data of PMBF

Comp.	PMBF
Structures	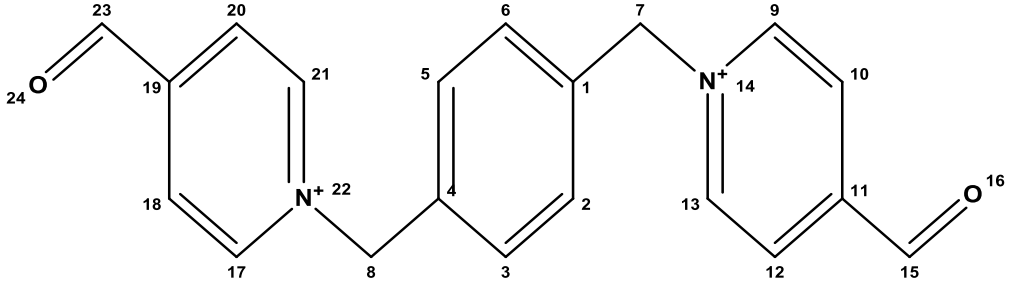
Mol. formula	$C_{20}H_{18}N_2O_2Br_2$
FT-IR (KBr) (cm^{-1})	3033 ν(C-H) arom, 2979 ν(C-H) aliph, 2764ν(C-H) aldehyde, 1659 ν(C=O) aldehyde, 1576 ν(C=C) Aromatic, 1252 ν(C-N)
^{1}H-NMR (ppm)	6.39 (s, 4H, $2CH_2$-N); 7.68 (d, 4H, Ar-H); 8.10 (d, 4H, Ar-H); 9.35 (d, 4H, Ar-H); 10.25 (s, 2H, 2CHO).
^{13}C-NMR (ppm)	62.3 (C7, C8); 125.8 (C10, C12, C18, C20); 130.1 (C2, C3, C5, C6); 136.1 (C1, C4); 145.3 (C9, C13, C17, C21); 147.2 (C11, C19), 190.3 (C15, C23).

3. RESULTS AND DISCUSSION

3.1. Synthesis of 1,1′-(1,4-Phenylenebis(methylene))-bis(4-formylpyridin-1-ium). The new 1,1′-(1,4-phenylenebis(methylene))bis(4-formylpyridin-1-ium) (PMBF) was synthesized utilizing the quaternization reactions of 4-pyridyne carboxaldehyde with α,α′-dibromo-*p*-xylene taking place in 1,2-dichloroethane as the solvent; 4-pyridyne carboxaldehyde was dissolved in a minimum volume of 1,2-dichloroethane, and α,α′-dibromo-*p*-xylene was then added directly to the solution in small portions. α,α′-Dibromo-*p*-xylene was added in an equimolar ratio (1:2). The synthesis route of PMBF is illustrated in Scheme 1.

3.2. Fourier Transform Infrared (FT-IR) Spectroscopy Analyses. The FT-IR spectrum, which revealed the structure of compound PMBF, exhibited peaks of ν(C−H) aromatic at 3033 cm^{-1}, ν(C−H) aliphatic at 2979 cm^{-1}, ν(C−H) aldehyde at 2764 cm^{-1}, ν(C═O) aldehyde at 1659 cm^{-1}, ν(C−N) at 1252 cm^{-1}, and ν(C═C) aromatic at 1576 cm^{-1}.[24] FT-IR spectrum data of PMBF are shown in Figure 1 and Table 1. Fourier transform infrared spectra were recorded using a KBr disc on a SHIMADZU FT-IR-8400, Japan, at the Faculty of Science, Chemistry Department, Al-Mustansiryah University, Iraq.

https://doi.org/10.1021/acsomega.3c02094
ACS Omega 2023, 8, 27079−27091

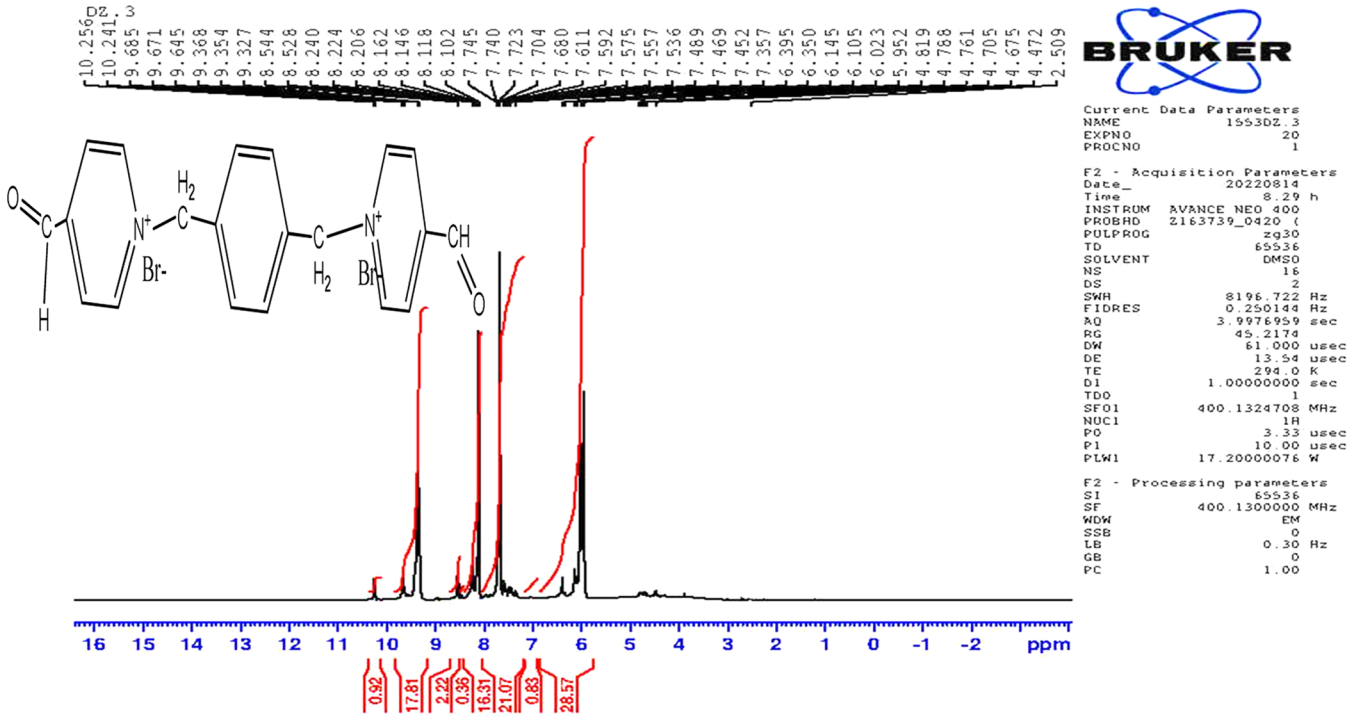

Figure 2. ^{1}H NMR spectrum of PMBF.

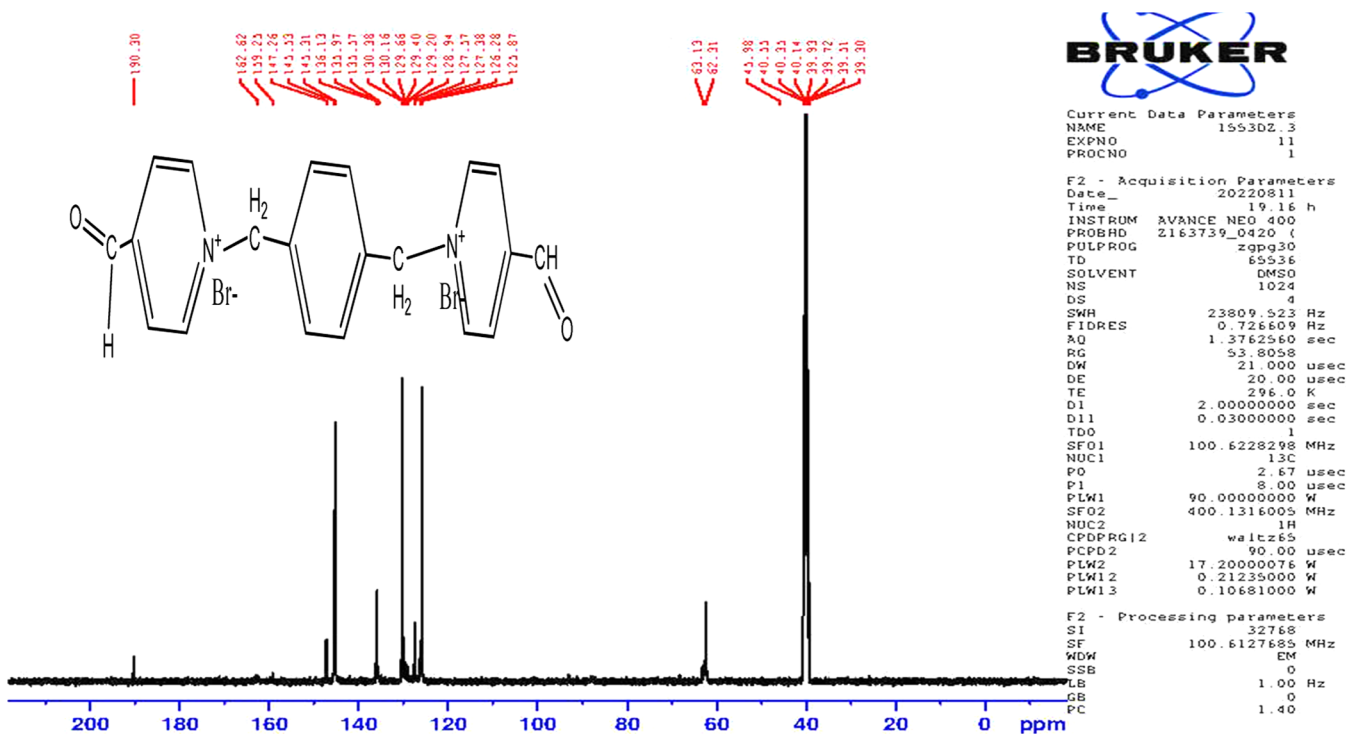

Figure 3. ^{13}C NMR spectrum of PMBF.

3.3. ^{1}H NMR Analyses. The ^{1}H NMR (DMSO) spectrum of PMBF showed signals of a multiplet at δ 7.3−7.4 due to the aromatic ring proton (m, 4H, Ar-H), a doublet at δ 8.1−8.54 due to the four protons of (4CH-COH), a doublet at δ 9.32−9.63 due to the four protons of (d, 4H, $-CH_2$-N), and a singlet at δ 9.64−9.68 due to the (s, 2H, −COH) aromatic.[24] ^{1}H NMR spectrum data of PMBF are shown in Figure 2 and Table 1.

3.4. ^{13}C NMR Analyses. The ^{13}C NMR (DMSO) spectrum of PMBF showed signals at 62.31 below to (C7,C8), signals at 125.87 below to (C10, C12, C18, C20), signals at 127.38 below to (C1, C2, C4, C5), signals at 136.16 below to (C9, C13, C17, C25), signals at 159.23 below to (C11, C19), signals at 190.3 below to (C15, C23) aromatic.[25] ^{13}C NMR spectrum data of PMBF are shown in Figure 3 and Table 1.

https://doi.org/10.1021/acsomega.3c02094
ACS Omega 2023, 8, 27079−27091

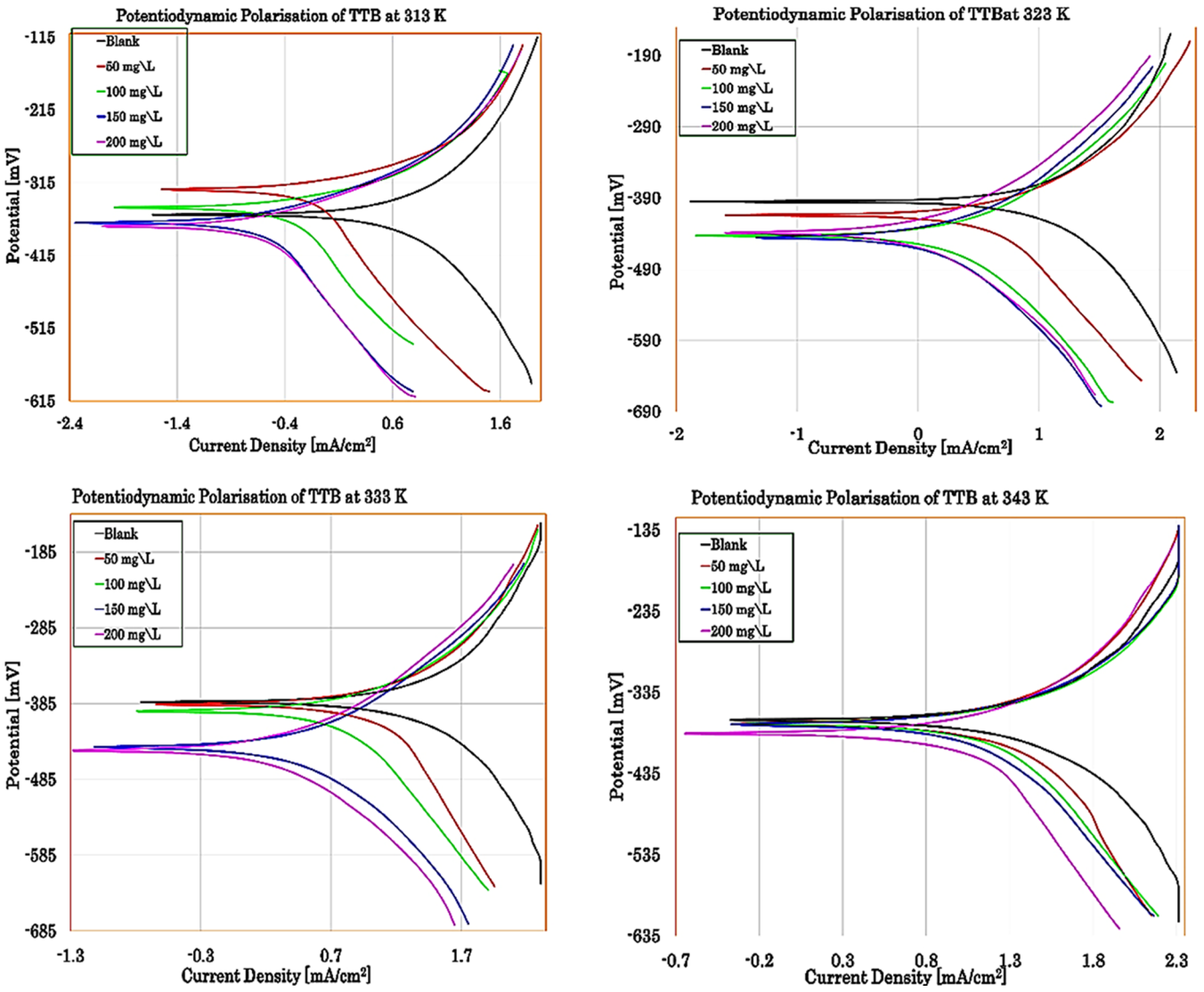

Figure 4. Tafel extrapolation curves for the dissolution of C101′8 in 17.5% HCl with and without variant doses of PMBF at altered temperatures.

Nuclear magnetic resonance, ^{1}H NMR, and ^{13}C NMR spectra were recorded using a Bruker UltraShield 300 mHz NMR system at Basrah University, Iraq using tetramethyl silane as the internal standard and DMSO-d_6 as the solvent.

3.5. PDP Measurements. The polarization curves for C1018 with and without various PMBF concentrations are displayed in Figure 4. The general shape of the potentiodynamic curve with and without PMBF is comparable. However, the increase in PMBF concentration inhibited the anodic and cathodic reactions, with a predominant cathodic effect. The extrapolation of the Tafel straight line allows the calculation of the corrosion current density (i_{corr}). Table 2 lists the parameters for anodic and cathodic Tafel slopes (β_a, β_c), inhibition efficiency (% IE), corrosion potential (E_{corr}), corrosion current density (i_{corr}), and inhibition potential. Equation 1 was used to determine the inhibitor efficiency %IE and degree of surface coverage (θ) from the measured (i_{corr}) values.

$$\%\,\mathrm{IE} = \theta \times 10 = \frac{i_{corr(free)} - i_{corr(i)}}{i_{corr(free)}} \times 100 \quad (1)$$

where $i_{corr(free)}$ is the uninhibited corrosion current and $i_{corr(i)}$ is the inhibited corrosion current. Figure 4 shows that after adding PMBF to a solution of 17.5% HCl, both the anodic and cathodic curves changed in the direction of less corrosion current, indicating the mixed nature of the inhibitor. The lower i_{corr} readings in the presence of PMBF show inhibitor molecule binding on the C1018 facet, which subsequently increases the %IE. The fact that the values of PMBF's β_a and β_c changed as the concentration of the inhibitor showed that PMBF regulated the anode and cathode reactions. PMBF is a mixed-type inhibitor, as evidenced by the lack of change in E_{corr} values in the attendance of the inhibitor compared to E_{corr} in the absence of the inhibitor (23.4 mV at 313 K).[25] This finding implies that PMBF is adsorbed by obstructing the reaction sites on the surface of C1018, reducing the amount of surface area accessible for hydrogen evolution (cathodic reaction) and metal dissolution (anodic reaction) without changing the process mechanism.

Higher PMBF inhibitor concentrations, as indicated by the provided parameters in Table 2, reduce the anodic and cathodic corrosion current densities. In comparison to the results obtained in the presence of various PMBF concen-

https://doi.org/10.1021/acsomega.3c02094
ACS Omega 2023, 8, 27079−27091

Table 2. Electrochemical Data Obtained from Tafel Plots for C1018 in 17.5% HCl with Different PMBF Concentrations at Various Temperatures

T (K)	concn ($\times 10^5$ M)	$E_{corr.}$ (mV vs. SCE)	i_{corr} (mA cm^{-2})	β_c (mV dec^{-1})	β_a (mV dec^{-1})	weight loss (g m^{-2}·day^{-1})	penetration loss (mm a^{-1})	corros. rate (mpy)	θ	IE %
313		−360.7 ± 2.6	10.37 ± 0.01	−254.5 ± 1.2	243.1 ± 1.2	2595.2	120.4	4739.0		
	10.51	−362.4 ± 2.9	0.239 ± 0.01	−391.2 ± 1.3	81.4 ± 1.5	59.9	2.8	109.5	0.977	97.7
	21.01	−370.6 ± 2.5	0.194 ± 0.01	−599 ± 1.5	75.9 ± 1.7	48.7	2.3	89.0	0.981	98.1
	31.52	−349.4 ± 3.6	0.179 ± 0.01	−650.4 ± 1.2	89.4 ± 1.5	44.8	2.1	81.9	0.983	98.3
	42.02	−347.5 ± 3.1	0.155 ± 0.01	−705.3 ± 1.6	77.3 ± 1.3	38.8	1.8	70.9	0.985	98.5
323		−397.6 ± 2.8	25.74 ± 0.01	−319.8 ± 1.1	324.9 ± 1.9	6441.5	298.8	11,762.6		
	10.51	−373.4 ± 3.9	0.509 ± 0.01	−481.1 ± 1.2	102 ± 1.7	127.4	5.9	232.7	0.980	98.0
	21.01	−376.8 ± 4.6	0.39 ± 0.01	−521.6 ± 1.4	91.6 ± 1.8	97.5	4.5	178.0	0.985	98.5
	31.52	−375.6 ± 4.1	0.32 ± 0.01	−344.4 ± 1.4	84.8 ± 2.0	80.2	3.7	146.5	0.988	98.8
	42.02	−369.7 ± 4.0	0.311 ± 0.01	−345.1 ± 1.3	77.2 ± 2.0	77.8	3.6	142.1	0.988	98.8
333		−387.4 ± 5.6	39.49 ± 0.01	−267.8 ± 1.6	286.9 ± 1.9	9874.5	458.0	18,031.5		
	10.51	−395.9 ± 5.8	0.909 ± 0.01	−413.1 ± 1.5	98.9 ± 1.8	228.5	10.6	417.3	0.977	97.7
	21.01	−385.4 ± 3.8	0.68 ± 0.01	−386.6 ± 1.5	96.7 ± 1.2	170.3	7.9	311.0	0.983	98.3
	31.52	−376.7 ± 4.7	0.587 ± 0.01	−343.8 ± 1.2	86.6 ± 1.5	146.8	6.8	268.1	0.985	98.5
	42.02	−374.1 ± 5.6	0.578 ± 0.01	−358.1 ± 1.4	89 ± 1.6	144.7	6.7	264.2	0.985	98.5
343		−372.8 ± 1.6	55.01 ± 0.01	−348 ± 1.2	335.7 ± 1.9	13,776.8	639.0	25,157.4		
	10.51	−401.4 ± 3.2	1.52 ± 0.01	−258 ± 1.8	98.2 ± 1.7	379.5	17.6	692.9	0.972	97.3
	21.01	−385.4 ± 5.6	1.23 ± 0.01	−327.5 ± 1.9	100.4 ± 1.6	308.3	14.3	563.0	0.978	97.8
	31.52	−381.5 ± 2.1	1.18 ± 0.01	−299.5 ± 1.7	93.7 ± 1.8	295.4	13.7	539.4	0.979	97.9
	42.02	−380.5 ± 4.9	1.15 ± 0.01	−296 ± 1.9	92.4 ± 1.5	288.9	13.4	527.6	0.979	97.9

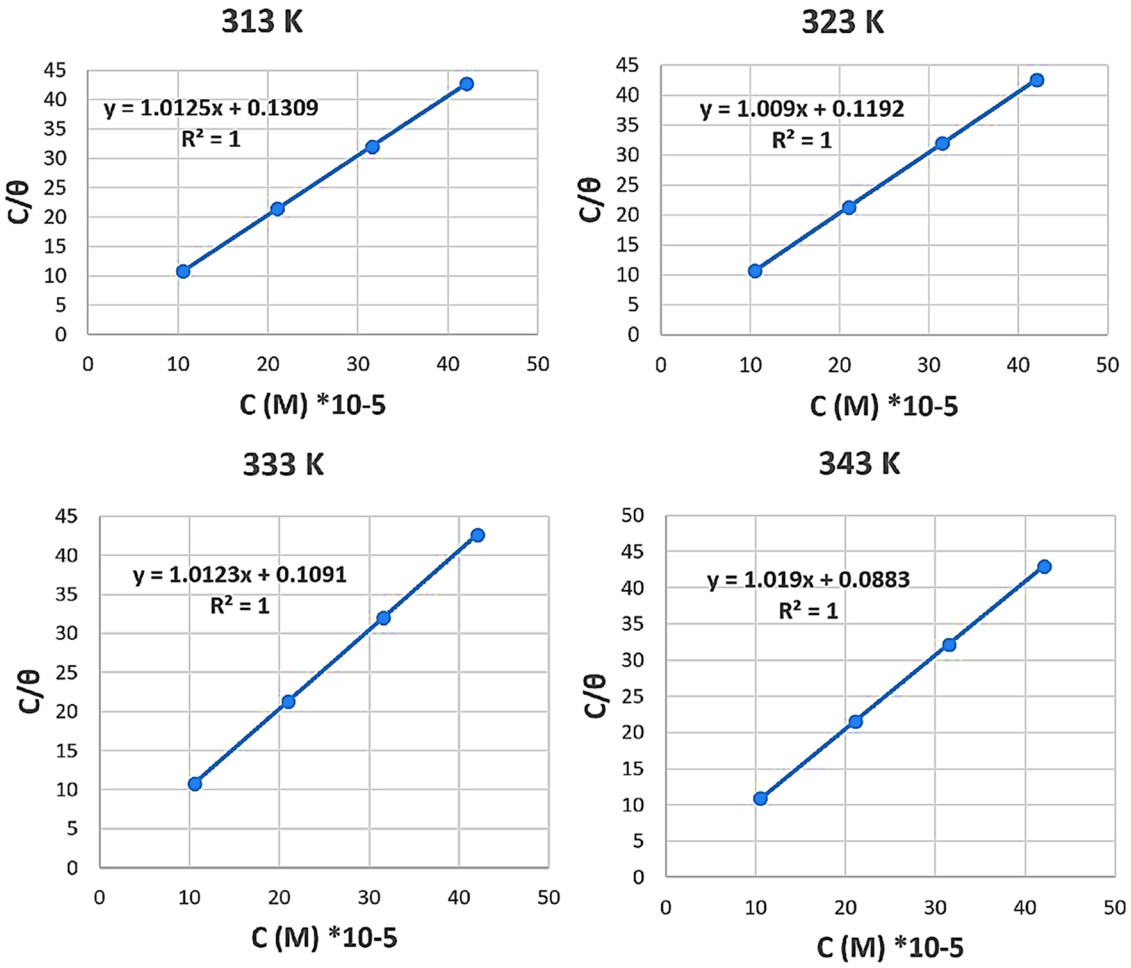

Figure 5. Langmuir adsorption isotherm of PMBF on C-steel in 17.5% HCl at different temperatures.

trations, the i_{corr} was the highest in the acidic blank solution at all temperatures. As the reaction temperature was increased, the i_{corr} increased at all tested inhibitor doses as the temperature impact was seen. For instance, the i_{corr} values

https://doi.org/10.1021/acsomega.3c02094
ACS Omega 2023, 8, 27079−27091

measured at 313 and 343 K in the presence of 42.02×10^{-5} M PMBF were 0.155 and 1.15 mA cm^{-2}, respectively. The rapid electrochemical reactions and metal disintegration at higher temperatures could be the cause of the significant increase in the current density (around 10 times).[26] The anodic and cathodic curves altered toward greater positive and negative potentials, respectively, in accordance with the obtained results, identifying PMBF as a mixed-type corrosion inhibitor.[27] As shown in Figure 4, the anodic and cathodic curves did not significantly change at increasing inhibitor concentrations. Inhibitors are described as mixed-type inhibitors unless there is an 85 mV potential shift between the blank and inhibited solutions, which is when they are classed as cathodic or anodic.[28,29] Indeed, at increased PMBF concentrations, the corrosion rates decreased, revealing a decreased affinity of C1018 for chloride ion adsorption. The excessive accumulation of inhibitor molecules and the resulting increase in electron density on the surface of C1018 accounted for this decrease. On the other hand, it was observed that at higher temperatures, the corrosion rate increases as a result of inhibitor molecules' desorption from the C1018 surface.[30] The %IE was determined to be 98.50% at 313 K and 42.02×10^{-5} M PMBF inhibitor. In terms of inhibitory effectiveness and surface coverage, larger PMBF concentrations result in greater surface coverage because of the accumulation of inhibitor molecules. The performance of the inhibitor was therefore markedly improved at the highest concentration of 42.02×10^{-5} M at all temperatures. Because corrosion occurs more quickly at higher temperatures, efficiency was also reduced.

3.6. Adsorption Studies and Thermodynamic Isotherms. To understand the mechanism of the adsorption of the PMBF to the metal surface, the adsorption isotherm provides details regarding the interactions between the species that have been attached to the reacted metal surface. The Langmuir, Temkin, Frumkin, and Freundlich isotherms are the most utilized adsorption isotherms. The best description of the adsorptive behavior was found to be the Langmuir adsorption isotherm (Figure 5). Langmuir isotherm states that the metal surface has a definite proportion of adsorption sites with one adsorbate and "Gibbs free energy of adsorption has the same value of sites, independent of the value of surface coverage".[31] Equation 2 describes the Langmuir adsorption isotherm.[32]

$$C/\theta = 1/K_{ads} + C \quad (2)$$

where C is the PMBF dose. K_{ads} is the adsorptive equilibrium constant (degree of adsorption). The strongly adsorbed inhibitor on the metal surface is indicated by a greater value of K_{ads}. A straight line is produced by the plot of C/θ vs. C in Figure 5, and the regression coefficient R^2 is nearly 1. This indicates that PMBF complied with the Langmuir isotherm in the current investigation and the molecules that have been adsorbed rarely interacted with one another. At lower temperatures, PMBF is readily and aggressively adsorbed onto the surface of C1018, as seen by the values of the equilibrium constant K_{ads} decreasing with increasing temperature. The free energy of adsorption was calculated using the relationships listed below.[33]

$$K_{ads} = 1/55.5 \exp(-\Delta G^{o}_{ads}/RT) \quad (3)$$

$$\Delta G^{o}_{ads} = -2.303RT \log(55.55\, K_{ads}) \quad (4)$$

$$\log K_{ads} = -\Delta H_{ads}/2.303RT + \Delta S_{ads}/2.303R + \log 1/55.55 \quad (5)$$

The dose of H_2O in solution in mol·L^{-1} is represented by the number 55.55 in the equations above. Table 3 presents the

Table 3. Thermodynamic Parameters ΔG°_{ads}, ΔH°_{ads}, and ΔS°_{ads} of the Adsorption of PMBF on C1018 at Various Temperatures

inhibitor	temp. (K)	K_{ads} (M^{-1})	$-\Delta G^{\circ}_{ads}$ (kJ mol^{-1})	ΔH°_{ads} (kJ mol^{-1})	ΔS°_{ads} (J mol^{-1} $K^{-1\prime}$)
PMBF	313	1595.48	29.65	10.84	0.129
	323	1762.88	30.87		
	333	1927.04	32.07		
	343	2326.08	33.57		

results of the Langmuir adsorption isotherm. The stability of the adsorbed layer on the metal surface and the spontaneity of the adsorption process are both guaranteed by the negative values of ΔG°_{ads}. The general rule is that at values of ΔG°_{ads} of up to -20 kJ mol^{-1} a charged metal and a charged molecule interacting electrostatically would be expected (physisorption), while those at or above -40 kJ mol^{-1} are linked to chemisorption as a result of the organic molecules sharing or transferring electrons to the metal surface to establish a coordinate type of bond. Given that the acquired ΔG°_{ads} values fall between the previously specified ranges, which is between -29.65 and -33.56 kJ mol^{-1}, this indicates mixed-type adsorption. The importance of K_{ads} in revealing the strength of bonding between the inhibitor and the C1018 coupon surface was observed (is indicated). Desorption of PMBF molecules from the surface of C1018 and a weak interaction are found to occur from K_{ads} decreasing at higher temperatures. The slope of the variation of $\log(K_{ads})$ vs. $1/T = (-\Delta H_{ads}/2.303R)$ is shown in Figure 6; ΔH_{ads} was found to be 10.84 kJ

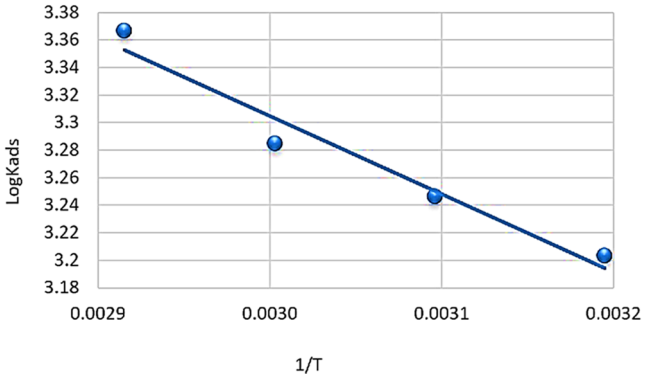

Figure 6. Plot of $\log K_{ads}$ against reciprocal of temperature values.

mol^{-1}. The presence of a positive result for ΔH_{ads} revealed that the inhibitor's adsorption mechanism is endothermic. When comparing the two processes, physisorption differs from chemisorption by the fact it has an exothermic value below -40 kJ mol^{-1}, while the adsorption heat of the chemisorption phenomenon is about -100 kJ mol^{-1}".[34] The standard adsorption heat used in this work ΔH°_{ads} equaled 10.84 kJ mol^{-1}, suggests that physical adsorption is preferred. The adsorption of PMBF on the surface of C1018 was associated

https://doi.org/10.1021/acsomega.3c02094
ACS Omega 2023, 8, 27079−27091

Table 4. Corrosion Kinetic Parameters for C1018 in 17.5% HCl in the Absence and Presence of Different Concentrations of PMBF

concn (×10^5 M)	temp. (K)	$i_{corr.}$ (mA cm^{-2})	A (molecules cm^{-2})	E_a* (kJ mol^{-1})	ΔH* (kJ mol^{-1})	$-\Delta S$* (J mol^{-1} K^{-1})
blank	313	10.3700	9.99319 × 10^{32}	48.799	46.076	0.077
	323	25.7400				
	333	39.4900				
	343	55.0100				
10.51	313	0.23933	2.09327 × 10^{32}	54.792	52.069	0.090
	323	0.50891				
	333	0.90925				
	343	1.5200				
21.01	313	0.19441	1.42602 × 10^{32}	54.812	51.689	0.094
	323	0.38958				
	333	0.68035				
	343	1.23				
31.52	313	0.17891	2.13143 × 10^{32}	55.826	53.103	0.090
	323	0.32041				
	333	0.58656				
	343	1.18				
42.02	313	0.15536	6.73728 × 10^{32}	59.105	56.382	0.081
	323	0.31134				
	333	0.57785				
	343	1.15				

with a decrease in system order, according to the positive value of standard adsorption entropy.

3.7. Corrosion Kinetics Studies. PDP measurements were performed in the temperature range of 313−343 K without and with various PMBF concentrations in order to examine the impact of temperature on the inhibitory efficiency of PMBF. The Arrhenius equation (eq 6) is the formula used to calculate the activation parameters of the dissolution process. Also, eq 7 for the transition state was utilized:[35]

$$\log(i_{corr}) = \log A - E^*_a/2.303RT \quad (6)$$

$$\log(i_{corr}/T) = \log(R/Nh) + \Delta S^*/2.303R - \Delta H^*/2.303RT \quad (7)$$

where i_{corr} is the corrosion current, E_a* is the energy of activation, R is the universal gas constant (8.314 J mol^{-1} K^{-1}), T is the temperature in K, A is the Arrhenius factor, h is Planck's constant (6.626 × 10^{-34} J·s), N is Avogadro's number (6.022 × 1023 mol^{-1}), ΔH* is the activation enthalpy, and ΔS* is the entropy of activation. The log i_{corr} vs. $1/T$ plot revealed a linear relationship with a slope of ($-E_a$*/2.303R) and an intercept of the extrapolated line of log A. Table 4 illustrates the results. From the plots of log i_{corr}/T vs. $1/T$, straight lines were obtained, which are presented in Figure 7 with a slope of ($-\Delta H$*/2.303R) and an intercept of [log(R/Nh) + (ΔS*/2.303R)], which were used to calculate the values of ΔH* and ΔS*, respectively. Figure 8 provides the Arrhenius charts for a temperature range of 313−343 K in 17.5% HCl. Based on the corrosion current measured values determined from polarization curves at various temperatures with and without of PMBF as a corrosion inhibitor (Arrhenius and transition states were applied).[36]

According to the activation kinetic parameters, at increasing inhibitor concentrations, the activation enthalpy increased, indicating a decrease in the corrosion rate. The higher activation energy values point to physisorption of the PMBF species onto the surface of C1018, allowing the corrosion

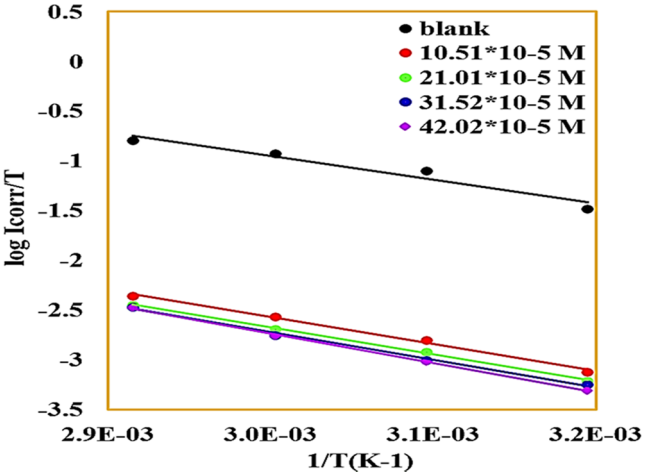

Figure 7. Transition state plot for C1018 in 17.5% HCl in the presence of different doses of PMBF.

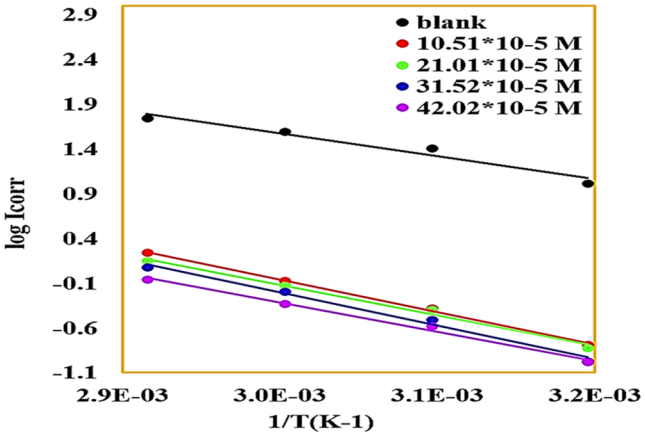

Figure 8. Arrhenius plot of C1018 in 17.5% HCl contains different concentrations of PMBF at different temperatures.

https://doi.org/10.1021/acsomega.3c02094
ACS Omega 2023, 8, 27079−27091

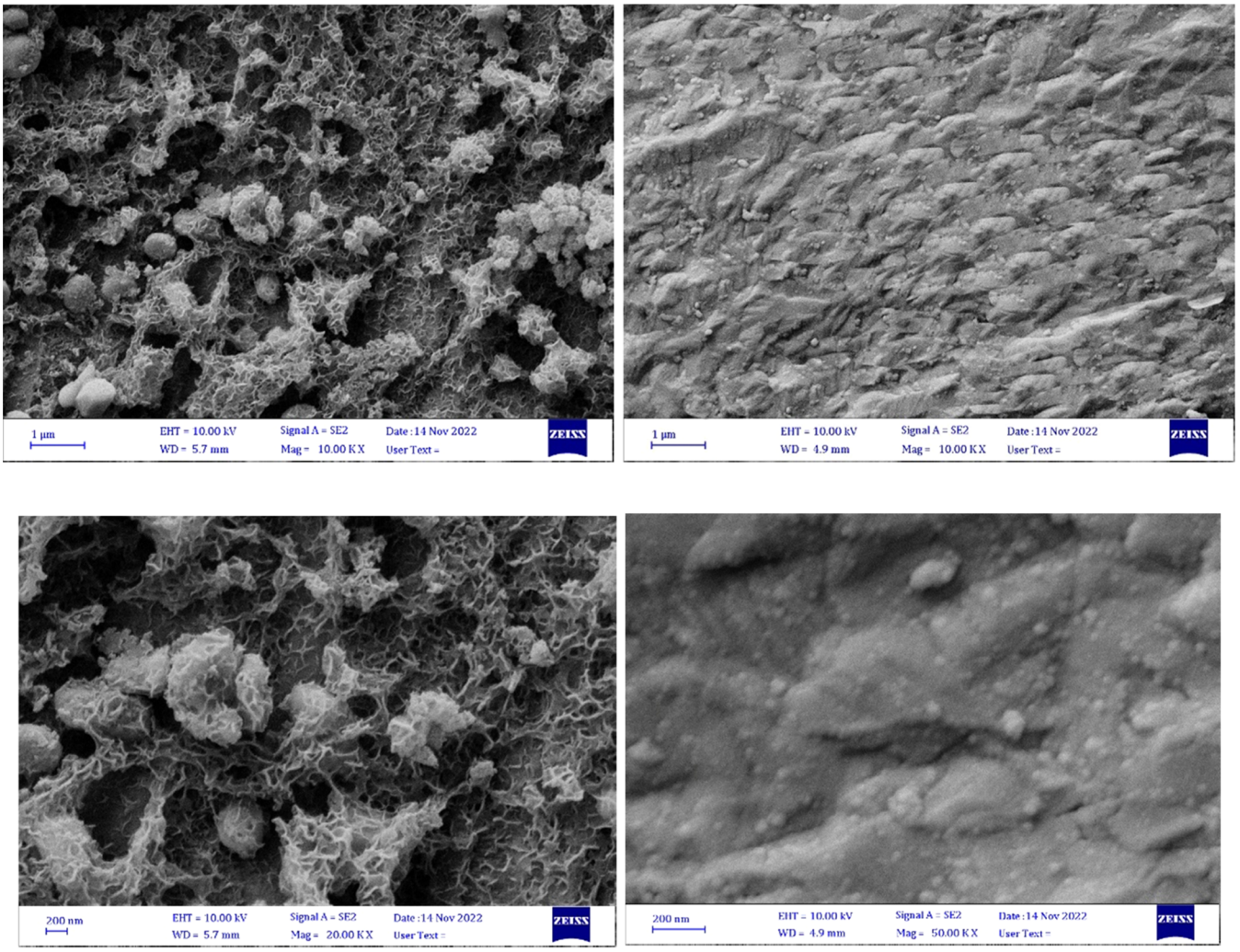

Figure 9. (a, b) SEM micrographs of C1018 in a 17.5% HCl solution at 313 K: (a) without PMBF and (b) in the presence of PMBF.

process's energy barrier to increase. The endothermic nature of the disintegration of C1018 is indeed reflected in the positive value of ΔH^*. The negative values of ΔS^* indicated that a larger order was created throughout the activation process. This can be accomplished through the production of an activated complex, which stands for association or fixation and results in a decrease in the system's degrees of freedom.

3.8. Scanning Electron Microscopy (SEM) Analyses. Figure 9a,b shows the SEM images of C1018 that corroded in 17.5% HCl with and without the PMBF inhibitor. The corroded surface of C1018 is demonstrated by the acid-dipped coupons (Figure 9a). The damaged body is evidence that hydrochloric acid has dissolved the iron that was present on the metal surface. In addition, the eroded holes can be found throughout the entire sample, verifying the acid attack on C1018. In contrast, a packed film layer was produced, as shown in Figure 9b, due to the adsorption of the layer by the synthetic PMBF inhibitor; the surface was smooth and free of pits. The inhibition process is made possible by the formation of a protective surface by the inhibitor on the metal surface. Hence, the inhibitor actively prevents acid corrosion from occurring on the C1018 surface.

3.9. Atomic Force Microscopy (AFM) Analyses. As shown in Figure 10a,b, using three-dimensional (3D) AFM, the surface roughness and topography of the C1018 coupons were examined. Characterization approaches at the nanoscale level. AFM is a reliable tool for quantifying surface roughness and assessing the effectiveness of corrosion inhibitors. Figure 10a depicts the pitted, corroded metal surface immersed in a 17.5% HCl solution without the PMBF inhibitor. In this situation, the R_q (root-mean-squared roughness), R_a (average roughness), and P−V (maximum peak-to-valley) height values observed for the C1018 surface are 68.25, 53.05, and 46.18 nm, respectively. These results imply that C1018 surface immersed in 17.5% HCl; has a rougher surface because it corrodes in an acidic environment. The C1018 surface following immersion in an acidic liquid containing 17.5% HCl is depicted in Figure 10b. The C1018 surface's R_q, R_a, and $P-V$ height values are 32.77, 24.28, and 31.37 nm, respectively. The R_q, R_a, and $P-V$ values were comparable to those in an uninhibited environment; height values were significantly lower in an inhibited environment. These parameters demonstrate a smoother surface due to the compact protective film of the Fe^{2+}−PMBF complex that forms on the metal surface and smoothens its surface and then prevents C1018 from corroding.

3.10. Quantum Chemical Calculations. Quantum chemical calculations have a significant impact on the design and development of corrosion inhibitors. The distribution of electrons and the molecule shape were precisely determined by the DFT theory. Quantum chemical computations were used

https://doi.org/10.1021/acsomega.3c02094
ACS Omega 2023, 8, 27079−27091

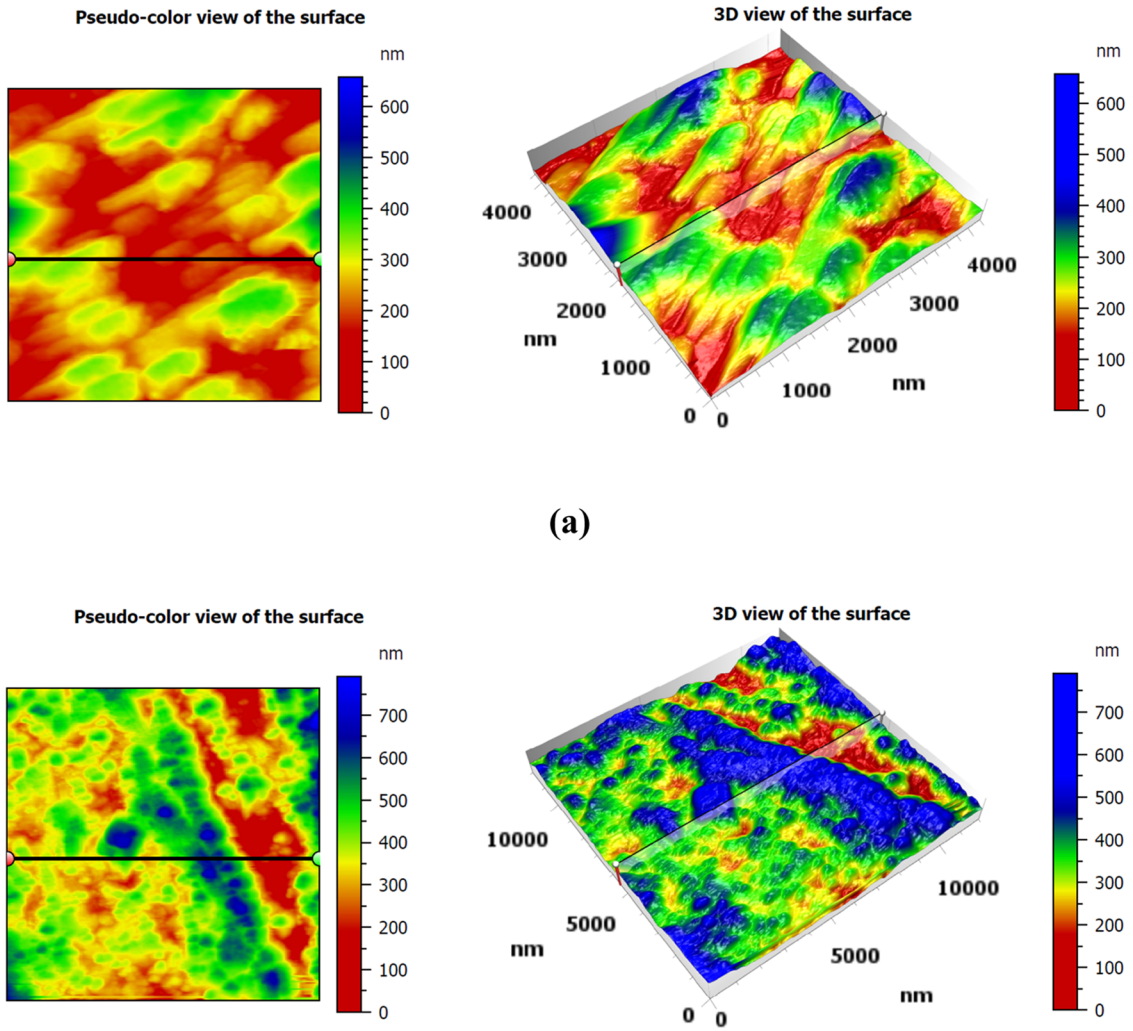

Figure 10. AFM images of the surface of (a) C1018 immersed in 17.5% HCl (blank) and (b) C-steel immersed in 17.5% HCl + PMBF inhibitor.

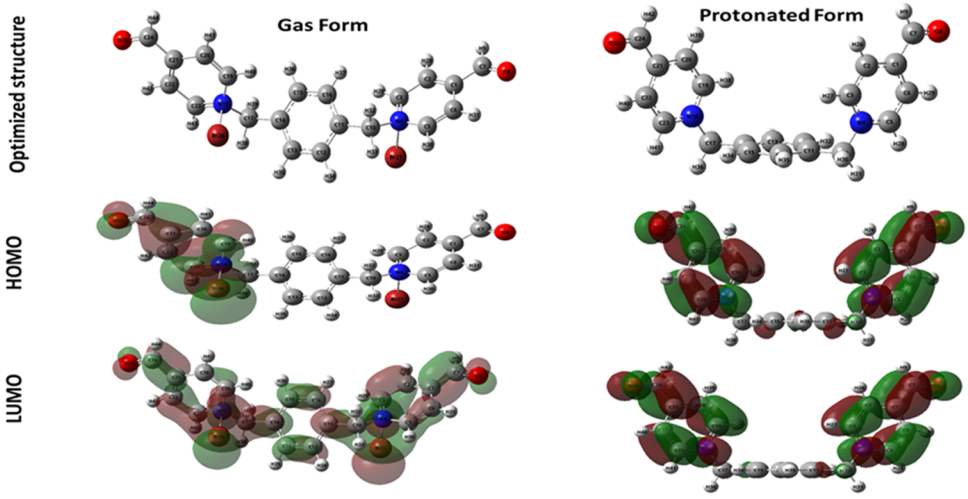

Figure 11. Frontier molecular orbital diagram of the investigated compound and optimized structure.

in this study to analyze the corrosion characteristics of an inhibitory molecule and the interaction between a metal. Quantum chemical descriptors, such as energy of the highest occupied molecular orbital (E_{HOMO}) and energy of the lowest unoccupied molecular orbital (E_{LUMO}), are popularly used, as shown in Figure 11. As shown in Table 5, the investigated inhibitor possessed the highest HOMO level energy at −4.278 eV and the lowest LUMO level energy at −1.102 eV in the protonated form, but in the case of the gas form, it had HOMO level energy and LUMO level energy at −3.121 and −1.322 eV, respectively. This illustrated that the inhibitor in the protonated form has high reactivity than in the gas form,

https://doi.org/10.1021/acsomega.3c02094
ACS Omega 2023, 8, 27079−27091

Table 5. Quantum Chemical Parameters of the Inhibitor in Protonated and Gas Forms

forms of the inhibitor	E_{HOMO}	E_{LUMO}	$\Delta E = E_{LUMO} - E_{HOMO}$	dipole moment
protonated form	−4.278	−1.102	1.588	9.231
gas form	−3.121	−1.322	1.799	9.111

producing high inhibitor efficiency. Several studies reported that lower ΔE values are associated with greater inhibitory efficacy. Through this result, the investigated protonated compound has low energy gap than in the gas form, which protects the metal from corrosion to a large extent in the protonated form. An aqueous solution of the inhibitor has dipole moments of 9.231 and 9.111 in protonated and gas forms. Strong dipole−dipole interactions with the C1018 surface are attributed to the inhibitor's high dipole moment. It is possible that the inhibitor increases the inhibition sites on the C1018 surface in a corrosive medium (15%).

3.11. Electrostatic Potential (ESP) Maps. According to Figure 12, the studied inhibitor has a transparent surface for total electron density and electrostatic potential (ESP) mapping. Sites and centers with negative and positive potentials were found using ESP pictures. A green-blue region corresponds to a positive potential that receives electrons from the metal surface, whereas a red-yellow region corresponds to a negative potential as oxygen atoms are responsible for donating electrons to the metal surface.

3.12. Monte Carlo Simulations. The inhibitor was preferentially adsorbed with the majority of the heteroatom parallel to Fe, as seen in the top and side views (Figure 13, left and right panels, respectively) (1 1 0). Thus, the surface area of contact between the inhibitor and Fe is increased (1 1 0). Larger molecules have greater surface areas, which would improve the effectiveness of their inhibition. As seen in Table 6, the inhibitor's negative adsorption energy points to stable/strong adsorption and chemical interaction with Fe(1 1 0). As electrons are given to the vacant d-orbitals of iron and oxygen and nitrogen atoms, protective coating forms on the metal surface (1 1 0). Also, we looked into stable adsorption arrangements of the compound under study on Fe(1 1 0) in the aqueous phase in gas and protonated forms. We concluded that adsorption is the mechanism through which corrosion inhibitors interact with metals based on the results shown in Figure 13 and Table 6. As a result, we concluded that the tested inhibitor would probably create a stable adsorption layer and guard Fe against corrosion.

3.13. Mechanisms of Corrosion. As already stated, adsorption on the metal surface is the initial step in an inhibitor's action mechanism in corrosive conditions. A few factors that affect adsorption include the inhibitor's chemical composition, the metal's nature and surface charge, the quantity and variety of adsorption sites, the type of aggressive electrolytes, and the interaction of the inhibitor's organic molecules with the metallic surface.[37] It is important to keep in mind that C1018 has a positive surface charge under acidic conditions[38−40] due to $E_{corr} - E_q = 0$ (zero charge potential) > 0,[41] which should typically prevent the adsorption of protonated species, which predominate for PMBF in acidic media. However, the capacity of some anions in solution (Cl^- and Br^-) to become specifically adsorbed on the positively charged metal surface is a crucial factor since the resulting surface charge modification greatly changes the nature of metal−inhibitor interactions. As a result, the surface of C1018 becomes negatively charged due to the selective adsorption of chloride and bromide ions. The dipoles of the surface compound are oriented with their negative ends toward the solution, preventing the acid solution from attaching directly to the C1018 surface, and ionized PMBF readily reaches the surface of the metal by electrostatic attraction. In order to connect the metal surface with PMBF, chloride and bromide ions serve as adsorption mediators. As a result, a composite adsorption film is created, with chloride and bromide ions sandwiched between the positively charged inhibitor component and the metal. This film works as a barrier facing the corrosive process. Also, it was revealed that the inhibitory efficiency decreases with increasing experimental temperature, as previously reported,[42] which indicates that higher temperatures can promote desorption of PMBF from the C1018 surface. Additionally, the tested inhibitor's electronic oxygen (O) doublet and the iron atoms' vacant orbitals can form coordination bonds, which strengthen the chemical adsorption. This is known as the "donation effect," which makes it possible for the tested inhibitor's oxygen (O) electronic doublet to bind to the iron atoms' vacant orbitals. Scheme 2 represents the schematic representation of this mechanism.

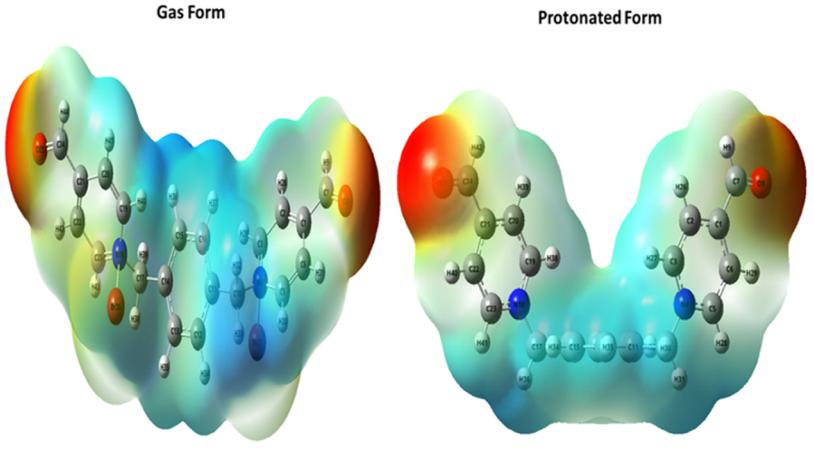

Figure 12. Transparent surface for ESP mapping of the investigated compound in gas and protonated forms.

https://doi.org/10.1021/acsomega.3c02094
ACS Omega 2023, 8, 27079−27091

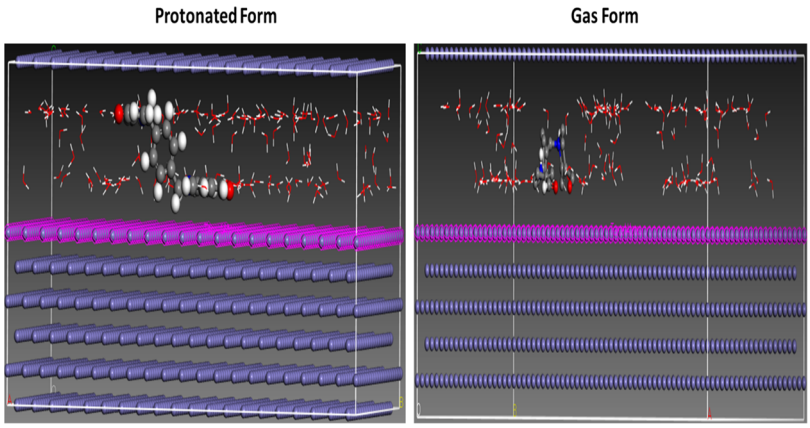

Figure 13. Most stable adsorption configuration for the studied inhibitor for Fe(1 1 0) in the aqueous phase.

Table 6. Parameters of Molecular Dynamic Simulations for the Studied Inhibitor on the Fe(1 1 0) Surface Obtained Using Monte Carlo Simulations

structure	E_{tot} (kJ mol^{-1})	E_{ads} (kJ mol^{-1})	E_{rigid} (kJ mol^{-1})	E_{def} (kJ mol^{-1})
Fe(1 1 0)-1 protonated form-1	−2210.513	−2211.179	−2282.548	71.369
Fe(1 1 0)-1 gas form	−2177.205	2557.613	−2300.350	−257.263

Scheme 2. Mechanism of Corrosion Inhibition

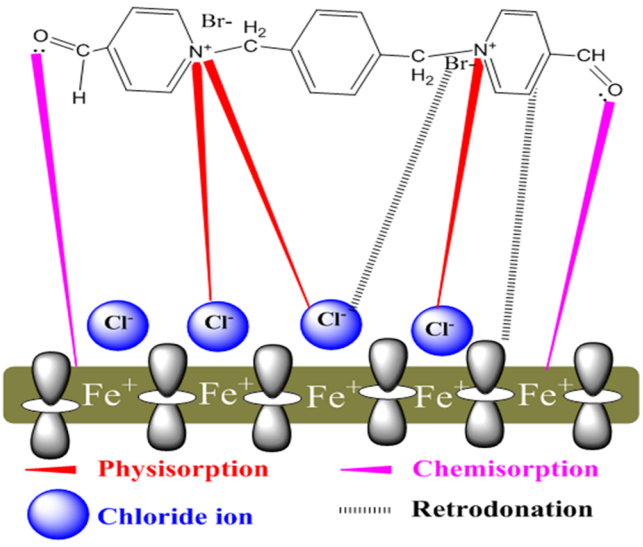

4. CONCLUSIONS

(1) The findings of the current investigation have shown that PMBF is an effective corrosion inhibitor for C1018 in a solution of 17.5% M hydrochloric acid.
(2) The corrosion inhibition efficiency increases with increasing inhibitor concentration and decreases by increasing the temperature.
(3) According to PDP measurements, PMBF functions as a mixed-type inhibitor, delaying both anodic and cathodic processes without altering the corrosion mechanism.
(4) The adsorption of PMBF on the C1018 surface obeys the Langmuir adsorption isotherm.
(5) The highest corrosion protection efficiency is approximately 98.79% at 323 K and 42.02 × 10^{-5} M concentration of PMBF.
(6) Electrochemical measurements and surface analyses show good agreement.

AUTHOR INFORMATION

Corresponding Author

Abd El-Aziz S. Fouda − *Department of Chemistry, Faculty of Science, Mansoura University, Mansoura 35516, Egypt;* orcid.org/0000-0002-3239-4417; Phone: +2 050 2365730; Email: asfouda@mans.edu.eg; Fax: +2 0502202264

Authors

Zaidoun K. Kuraimid − *Department of Chemistry, Faculty of Science, Mansoura University, Mansoura 35516, Egypt*

Dawood S. Abid − *College of Education for Pure Science, Basra University, Basra 61004, Iraq*

Complete contact information is available at: https://pubs.acs.org/10.1021/acsomega.3c02094

Notes

The authors declare no competing financial interest.

ACKNOWLEDGMENTS

This study was financially supported by the Department of Chemistry, Faculty of Science, Mansoura University, Egypt.

REFERENCES

(1) Njokua, D. I.; Chidiebere, M. A.; Oguzie, K. L.; Ogukwe, C. E.; Oguzie, E. E. Corrosion inhibition of mild steel in hydrochloric acid solution by the leaf extract of Nicotiana tabacum. *Adv. Mater. Corros.* **2013**, *2*, 54−61.
(2) Rajeev, P.; Surendranathan, A. O.; Murthy, C. S. N. Corrosion mitigation of the oil well steels using organic inhibitors−a review. *J. Mater. Environ. Sci.* **2012**, *3*, 856−869.
(3) Yang, H.-M. Role of organic and eco-friendly inhibitors on the corrosion mitigation of steel in acidic environments—A state-of-art review. *Molecules* **2021**, *26*, 3473.
(4) Ashassi-Sorkhabi, H.; Seifzadeh, D.; Hosseini, M. G. EN, EIS and polarization studies to evaluate the inhibition effect of 3H-phenothiazin-3-one, 7-dimethylamin on mild steel corrosion in 1 M HCl solution. *Corros. Sci.* **2008**, *50*, 3363−3370.
(5) Goni, L. K. M. O.; Jafar, M. A.; Mazumder, M. A.; Quraishi, M. Mizanur Rahman, Bioinspired heterocyclic compounds as corrosion

inhibitors: a comprehensive review. *Chem. - Asian J.* **2021**, *16*, 1324−1364.
(6) Iroha, N.; Maduelosi, N. Pipeline steel protection in oil well acidizing fluids using expired pharmaceutical agent. *Chem. Int.* **2020**, *6*, 267−276.
(7) Riggs, O. L.; Hurd, R. M. Temperature coefficient of corrosion inhibition. *Corrosion* **1967**, *23*, 252−260.
(8) Obot, I. B.; Solomon, M. M.; Umoren, S. A.; Suleiman, R.; Elanany, M.; Alanazi, N. M.; Sorour, A. A. Progress in the development of sour corrosion inhibitors: Past, present, and future perspectives. *J. Ind. Eng. Chem.* **2019**, *79*, 1−18.
(9) Palanisamy, G. Corrosion inhibitors. *Corros. Inhib.* **2019**, 1−24.
(10) Goyal, M.; Kumar, S.; Bahadur, I.; Verma, C.; Ebenso, E. E. Organic corrosion inhibitors for industrial cleaning of ferrous and non-ferrous metals in acidic solutions: A review. *J. Mol. Liq.* **2018**, *256*, 565−573.
(11) Li, X.; Brownawell, B. J. Quaternary ammonium compounds in urban estuarine sediment environments-a class of contaminants in need of increased attention? *Environ. Sci. Technol.* **2010**, *44*, 7561−7568.
(12) Avdeev, Y. G.; Nenasheva, T. A.; Frolova, L. V.; Marshakov, A. I.; Kuznetsov, Y. I. Cathodic reduction of hydrogen on low-carbon steel in solutions of mineral acids containing nitrogen-containing organic compounds. *Int. J. Corros. Scale Inhib.* **2021**, *10*, 262−283.
(13) Quraishi, M. A.; Jamal, D. Corrosion Inhibition by Fatty Acid Oxadiazoles for Oil Well Steel (N-80) and Mild Steel. *Mater. Chem. Phys.* **2001**, *71*, 202−205.
(14) Frenier, W. W.; Growcock, F. B.; Lopp, V. R. Mechanisms of Corrosion Inhibitors Used in Acidizing Wells. *SPE Prod. Eng.* **1988**, *3*, 584−590.
(15) Migahed, M. A.; Nassar, I. F. Corrosion Inhibition of Tubing Steel during Acidization of Oil and Gas Wells. *Electrochim. Acta* **2008**, *53*, 2877−2882.
(16) Zhang, C.; Zahedi Asl, V.; Lu, Y.; Zhao, J. Investigation of the corrosion inhibition performances of various inhibitors for carbon steel in CO_2 and CO_2/H_2S environments. *Corros. Eng., Sci. Technol.* **2020**, *55*, 531−538.
(17) Zhang, C.; Zhao, J. Effects of pre-corrosion on the corrosion inhibition performance of three inhibitors on Q235 steel in CO_2/H_2S saturated brine solution. *Int. J. Electrochem. Sci.* **2017**, *12*, 9161−9179.
(18) Zhang, C.; Zhao, J. Synergistic inhibition effects of octadecylamine and tetradecyl trimethyl ammonium bromide on carbon steel corrosion in the H_2S and CO_2 brine solution. *Corros. Sci.* **2017**, *126*, 247−254.
(19) Jalab, R.; Saad, M. A.; Sliem, M. H.; Abdullah, A. M.; Hussein, I. A. An Eco-Friendly Quaternary Ammonium Salt as a Corrosion Inhibitor for Carbon Steel in 5 M HCl Solution: Theoretical and Experimental Investigation. *Molecules* **2022**, *27*, 6414.
(20) Wang, Y.; Yang, Z.; Zhan, F.; Yu, Z. L.; Han, C.; Wang, X.; Chen, W.; Ding, M.; Wang, R.; Jiang, Y. Indolizine quaternary ammonium salt inhibitors part II: a reinvestigation of an old-fashioned strong acid corrosion inhibitor phenacyl quinolinium bromide and its indolizine derivative. *New J. Chem.* **2018**, *42*, 12977−12989.
(21) Hegazy, M. A.; Abdallah, M.; Awad, M. K.; Rezk, M. Three novel di-quaternary ammonium salts as corrosion inhibitors for API X65 steel pipeline in acidic solution. Part I: experimental results. *Corros. Sci.* **2014**, *81*, 54−64.
(22) Ks, Y.; Mj, U. Corrosion inhibition efficiency of newly synthesized quaternary ammonium salt in 1M HCl. *Indian J. Chem. Technol.* **2022**, *29*, 68−74.
(23) ASTM G1-3, Standard Practice for Preparing, Cleaning, and Evaluating Corrosion Test Specimens.
(24) Shriner, R. L.; Hermann, C. K. F.; Morrill, T. C.; Curtin, D. Y.; Fuson, R. C. *The Systematic Identification of Organic Compounds*; John Wiley & Sons, 2003.
(25) Murulana, L. C.; Kabanda, M. M.; Ebenso, E. E. Experimental and theoretical studies on the corrosion inhibition of mild steel by some sulphonamides in aqueous HCl. *RSC Adv.* **2015**, *5*, 28743−28761.
(26) Sliem, M. H.; El Basiony, N. M.; Zaki, E. G.; Sharaf, M. A.; Abdullah, A. M. Corrosion inhibition of mild steel in sulfuric acid by a newly synthesized Schiff base: an electrochemical, DFT, and Monte Carlo simulation study. *Electroanalysis* **2020**, *32*, 3145−3158.
(27) Bashir, S.; Lgaz, H.; Chung, I.-M.; Kumar, A. Potential of Venlafaxine in the inhibition of mild steel corrosion in HCl: insights from experimental and computational studies. *Chem. Pap.* **2019**, *73*, 2255−2264.
(28) Parveen, M.; Mobin, M.; Zehra, S.; Aslam, R. L-proline mixed with sodium benzoate as sustainable inhibitor for mild steel corrosion in 1M HCl: An experimental and theoretical approach. *Sci. Rep.* **2018**, *8*, No. 7489.
(29) Amin, M. A.; Khaled, K. F.; Fadl-Allah, S. A. Testing validity of the Tafel extrapolation method for monitoring corrosion of cold rolled steel in HCl solutions−experimental and theoretical studies. *Corros. Sci.* **2010**, *52*, 140−151.
(30) Abd-Elaal, A. A.; Elbasiony, N. M.; Shaban, S. M.; Zaki, E. G. Studying the corrosion inhibition of some prepared nonionic surfactants based on 3-(4-hydroxyphenyl) propanoic acid and estimating the influence of silver nanoparticles on the surface parameters. *J. Mol. Liq.* **2018**, *249*, 304−317.
(31) Fouda, A. S.; Abd El-Maksoud, S. A.; El-Hossiany, A.; Ibrahim, A. Corrosion protection of stainless steel 201 in acidic media using novel hydrazine derivatives as corrosion inhibitors. *Int. J. Electrochem. Sci.* **2019**, *14*, 2187−2207.
(32) Ahamad, I.; Quraishi, M. A. Mebendazole: new and efficient corrosion inhibitor for mild steel in acid medium. *Corros. Sci.* **2010**, *52*, 651−656.
(33) Zarrouk, A.; Hammouti, B.; Zarrok, H.; Al-Deyab, S. S.; Messali, M. Temperature effect, activation energies and thermodynamic adsorption studies of L-cysteine methyl ester hydrochloride as copper corrosion inhibitor in nitric acid 2M. *Int. J. Electrochem. Sci.* **2011**, *6*, 6261−6274.
(34) Martinez, S.; Stern, I. Thermodynamic characterization of metal dissolution and inhibitor adsorption processes in the low carbon steel/mimosa tannin/sulfuric acid system. *Appl. Surf. Sci.* **2002**, *199*, 83−89.
(35) Nambiar, N. K.; Brindha, D.; Punniyakotti, P.; Venkatraman, B. R.; Angaiah, S. Derris indica leaves extract as a green inhibitor for the corrosion of aluminium in alkaline medium. *Eng. Sci.* **2021**, *17*, 167−175.
(36) Morad, M. S.; El-Dean, A. M. K. 2, 2′-Dithiobis (3-cyano-4, 6-dimethylpyridine): A new class of acid corrosion inhibitors for mild steel. *Corros. Sci.* **2006**, *48*, 3398−3412.
(37) Li, X.; Deng, S.; Fu, H. Triazolyl blue tetazolium bromide as a novel corrosion inhibitor for steel in HCl and H2SO4 solutions. *Corros. Sci.* **2011**, *53*, 302−309.
(38) Banerjee, G.; Malhotra, S. N. Contribution to adsorption of aromatic amines on mild steel surface from HCl solutions by impedance, UV, and Raman spectroscopy. *Corrosion* **1992**, *48*, 10−15.
(39) Wahdan, M. H.; Hermas, A. A.; Morad, M. S. corrosion inhibition of carbon steels by propargyl triphenylphosphonium bromide in H2SO4 solution. *Mater. Chem. Phys.* **2002**, *76*, 111−118.
(40) Librini, M.; Lagrenee, M.; Vezin, H.; Gengembre, L.; Bentiss, F. Electrochemical and quantum chemical studies of new thiadizole derivatives adsorption on mild steel in normal HCl medium. *Corros. Sci.* **2005**, *47*, 485−505.
(41) Luo, H.; Guan, Y. C.; Han, K. N. Corrosion inhibition of a mild steel by aniline and alkylamines in acidic solutions. *Corrosion* **1998**, *54*, 721−731.
(42) Li, X.; Deng, S.; Fu, H.; Mu, G. Inhibition effect of 6-benzylaminopurine on the corrosion of cold rolled steel in H2SO4 solution. *Corros. Sci.* **2009**, *51*, 620−634.

https://doi.org/10.1021/acsomega.3c02094
ACS Omega 2023, 8, 27079−27091